PERGAMON

International Journal of Solids and Structures 37 (2000) 5009–5032

INTERNATIONAL JOURNAL OF SOLIDS and STRUCTURES

www.elsevier.com/locate/ijsolstr

An incrementally continuous deformation theory of plasticity with unloading

R. Peek

Shell International Exploration and Production, Rijswijk, The Netherlands

Received 25 January 1999; in revised form 3 August 1999

Abstract

For predictions of plastic buckling, and especially postbuckling behaviour and imperfection sensitivity it is desirable to have a plasticity theory that combines some of the desired characteristics of both the flow and deformation theories of plasticity. For this purpose a way to include unloading within a deformation theory of plasticity is given that preserves the incremental continuity of the resulting constitutive equations. This can only be achieved by allowing plastic deformations to occur within the yield surface. Such plastic deformations are controlled by a parameter m, which describes how rapidly the possibility of such plastic deformations disappears as the stress state moves away from the yield surface. A finite strain version of the formulation is given. The approach can be implemented with minimal changes to an elastic predictor – radial return algorithm for the flow theory of plasticity, by changing the elastic predictor phase only. For tests involving thick-walled ($D/t \approx 10$) cylinders with known axisymmetric imperfections under axial compression, this new deformation theory overpredicted the concertina wrinkling type deformations for a given amount of applied axial shortening, whereas the flow theory underpredicted these wrinkling deformations in some cases.

Keywords: Plasticity; Pipe; Bifurcation; Buckling corner theory; Flow theory; Deformation theory

1. Motivation

It is well known that for problems of plastic buckling, the flow theory of plasticity can lead to calculated bifurcation buckling loads that are too high, whereas the deformation theory leads to bifurcation loads that are more in line with the experimental observations (Hutchinson, 1974; Bushnell, 1982; El-Ghazaly and Sherbourne, 1985; Giezen, 1988; Blachut et al., 1996). When examined in terms of strains at bifurcation the flow/deformation theory differences, can become quite large, as shown in Fig. 1,

E-mail address: r.peek@siep.shell.com (R. Peek).

0020-7683/00/$ - see front matter
PII: S0020-7683(99)00294-2

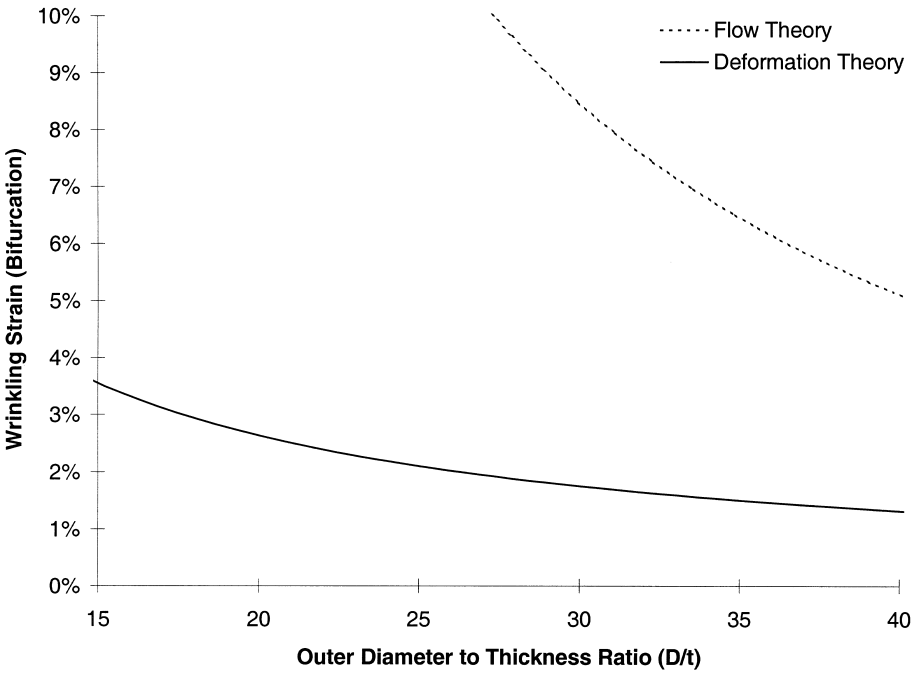

Fig. 1. Bifurcation strains for axisymmetric bucking of cylinders under axial compression based on the small-strain solution of Batterman (Batterman, 1965). (Poisson's ratio is 0.3, and stress–strain curve is defined in Eq. (13).)

based on Batterman's result (Batterman, 1965) for axisymmetric bifurcation buckling of a cylinder under axial load. In a number of practical applications it is not so much the buckling load, that is of importance, but rather the deformation capacity. For instance for reeling of pipelines one is interested in how far one can bend a pipe without wrinkling it. Also straight, high-temperature flowlines may wrinkle under axial compression, due to thermal strains large enough to cause yielding of the material, and the potential for the plastic deformations to concentrate in weaker areas of the pipe, where the buckling load may be exceeded. Therefore, errors in predictions such as those in Fig. 1, are not acceptable.

The reason for the flow/deformation theory differences is the sudden change in direction of the stress path at bifurcation buckling. Indeed for a broad range of plastic bifurcation problems, the stress path is normal to the yield surface, but upon bifurcation buckling it changes to one tangent to the yield surface (Hutchinson, 1974)[1]. For such non-proportional paths the flow and deformation theories predict different response of the material. This is illustrated in Fig. 2 by considering a loading path OABC in deviatoric stress space. The corresponding strain path is OABC for the flow theory of plasticity, but OABC' for the deformation theory. On the portion BC of the loading path, which is tangent to the yield surface, the behaviour is elastic for the flow theory but inelastic for the deformation theory. This is because the deformation theory does not include the path dependence, so that loading path OABC must produce the same final strain as a direct loading path OC. As a result for the deformation theory, a loading path tangent to the yield surface is associated with a "rotation" of the plastic strain tensor

[1] This applies for the neutral loading point from Hill's theory of bifurcation in the plastic range as described for instance in (Hutchinson, 1974).

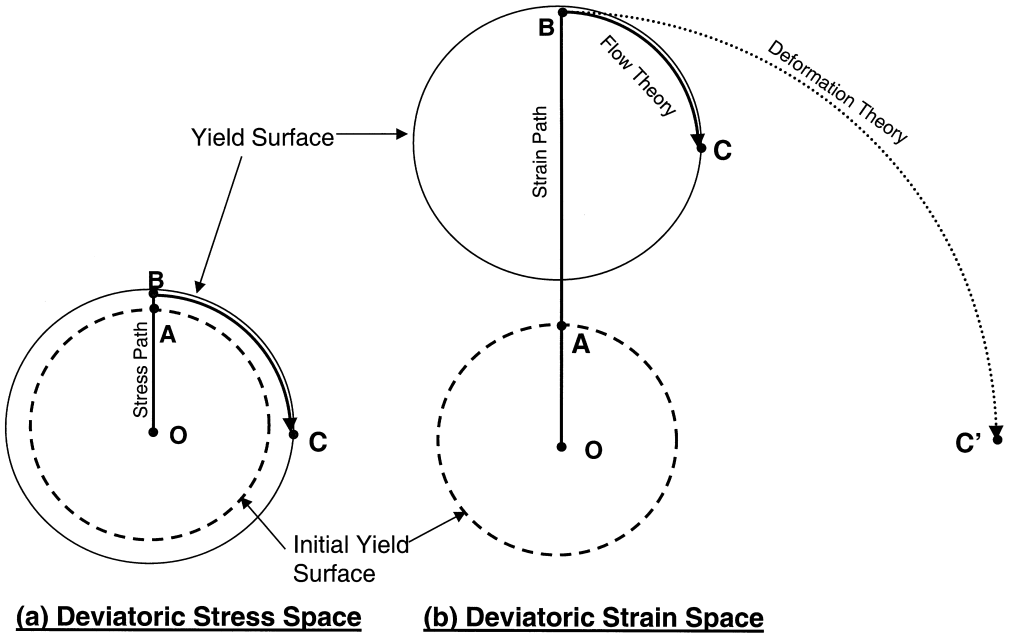

Fig. 2. Loading paths and yield surface locations for J2 flow and deformation theories of plasticity. For a given stress path OABC, the strain path is OABC for the flow theory, but it is OABC' for the deformation theory.

leading to the significantly more compliant material response. Indeed, the incremental moduli in the direction tangent to the yield surface are the elastic values for the flow theory, but the secant values for the deformation theory. It is this extra compliance for the deformation theory that leads to the better agreement with experimental results.

Of course, it is mainly the bifurcation buckling predictions for which the danger of using the flow theory is well-known. However, by choosing a sufficiently small imperfection buckling can be made to initiate arbitrarily close to the bifurcation point. Therefore, when the bifurcation buckling prediction is too high, the buckling load for the imperfect system will also be too high, for a sufficiently small imperfection. Granted that the phrase "sufficiently small" is here applied in a mathematical sense. From an engineering point of view imperfections may never be "sufficiently small". Nevertheless, the difference between the bifurcation predictions for the flow and deformation can be so large, that the prudent designer does well not to rely only on the flow theory, and its potentially unconservative predictions, even when some imperfections are involved.

The deformation theory also has some drawbacks. Although it results in generally better bifurcation buckling predictions, a true deformation theory does not account for elastic unloading of the material, since path dependent effects are not included. This is important, because of the known influence of elastic unloading on the postbifurcation behaviour. It is known that in almost all cases[2] involving bifurcation in the plastic range, elastic unloading begins immediately after bifurcation (Hutchinson, 1974), and it is for this reason that the bifurcated branches involve an initially increasing load. A true

[2] In Hutchinson's words (Hutchinson, 1974) an example could be "contrived" in which this is not the case. Such an example might be a Shanley column in which one of the springs is nonlinear elastic, but the other is elasto-plastic with the same stress–strain curve for plastic loading.

deformation theory will not predict this phenomenon. In view of the connection between postbifurcation behaviour and imperfection sensitivity, it is doubtful whether such a true deformation theory would give the right picture of the imperfection sensitivity of an elasto-plastic structure.

Unloading can be included within a deformation theory of plasticity, but this leads to a constitutive law involving discontinuities and/or ambiguities in the response. In particular the resulting incremental stress–strain relations become discontinuous at the loading/unloading boundary. This is not only physically unrealistic, but can lead to severe convergence difficulties in numerical computations.

This paper provides an approach to overcome the above-described drawbacks of both the flow and deformation theories. It is by no means the only way out of the dilemma, but it appears to be the simplest one available to date.

The resulting Incrementally Continuous deformation theory with Unloading (ICU deformation theory) can be implemented with minimal changes to an algorithm based on the standard flow theory. Furthermore, it has the following attributes:

(i) For proportional loading, unloading and reverse loading, it coincides with the flow theory of plasticity.
(ii) Bifurcation buckling predictions coincide with those of the deformation theory of plasticity for cases when the prebuckling solution involves proportional loading.
(iii) The theory is incrementally continuous and bilinear, and, as a result, no extra difficulties in the numerical solution procedures are introduced.

2. Background

The above-described drawbacks of both the flow and deformation theories have not only long been recognised, but a considerable amount of work has focused on finding a way out of this dilemma. A clear argument countering the objections to the deformation theory of plasticity has been put forward by Sanders (1954). He shows that if the von Mises yield surface is replaced by a number of planar yield surfaces that harden independently, then under certain restrictions the behaviour is path independent, and, as a result, the applicable incremental moduli are those of the deformation theory. Thus, Sanders created a physically more realistic model with the "right" incremental moduli for total plastic loading. (Total plastic loading occurs when yielding occurs on all active slip surfaces for which an active slip plane is one that is in contact with the current stress state.) This model is appealing because of its simplicity and the natural way in which it resolves the drawbacks of both the flow and deformation theories. However, in view of the large number of yield surfaces involved, it is not practical for finite element computations.

An approach more suitable for finite element computations is the "phenomenological corner theory" of Christofersen and Hutchinson (1979). In this theory the current stress state is at the vertex of a cone pushed out from the yield surface during strain hardening. For stress increments that return into this cone, the behaviour is elastic. Stress increments involving plastic loading may fall either in a total loading cone, where the incremental moduli of the deformation theory of plasticity apply, or in a transition region between the total loading and elastic unloading cones. For this transition region, the incremental moduli are defined by means of a transition function. This corner theory overcomes the above-described drawbacks of both the flow and the deformation theories, but not without a price: the resulting theory is more complicated than the standard flow and deformation theories. The stress–strain relation becomes incrementally nonlinear (rather than incrementally bilinear, as for standard plasticity theories), which can lead to convergence difficulties (Giezen, 1988). Finally experimental data to support

a clear definition of the transition function are not available and difficult to obtain (Hecker, 1976). Although this corner theory has seen a number of applications, mainly in the hands of researchers (Needleman and Tvergaard, 1982; Tvergaard, 1983; Triantafyllidis, 1985; Giezen, 1988), it seems that some of the difficulties associated with it have discouraged its more wide-spread use.

Despite the difficulties of the phenomenological corner theory, it does overcome the above-described drawbacks of both the flow and deformation theories. The intent here is not to present a competing approach. The ICU deformation theory proposed herein is essentially a special case of the corner theory, in which the corner in the yield surface becomes a needle, the total loading cone becomes a total loading halfspace. However, as will be seen, the development and implementation of this ICU deformation theory is much simpler than that of the corner theory.

3. Review of the deformation and flow theories of plasticity

The intent of this review is not to reiterate very well known theories. Rather it is to present them in such a form, that formulating the new ICU deformation theory becomes a trivial and obvious step. Although in the form stated here, the standard results might not be instantly recognised, they are fully equivalent to the formulation in (Hutchinson, 1973), which is also quoted in (Needleman and Tvergaard, 1977), where it is attributed to unpublished work by B. Budiansky. This is based on a generalisation of a small strain theory to finite strains in which the stress increment of the small strain theory is replaced by the Jauman rate of the Kirchhoff stress, and the strain increment of the small strain theory becomes the rate of deformation tensor. Such generalisation to finite deformations is applied to the small strain versions of both the flow and the deformation theories. This does lead to some path dependency in the elastic range (i.e. hypoelastic behaviour rather than hyperelastic behaviour), but the degree of path dependency should be small as long as the elastic strains are small. When the generalisation-to-finite-strains procedure is applied to a path independent deformation theory of plasticity, the resulting large strain deformation theory of plasticity can include more significant path dependence. Thus, when applied to a hyperelastic small-strain deformation theory of plasticity this generalisation-to-finite-strains approach will yield hypoelastic finite-strain deformation theory of plasticity. Nevertheless, it is hypoelastic deformation theory of plasticity that is used as a starting point here. According to Needleman and Tvergaard (1977) the path dependence of this theory only arises when there is a change of the principal axes of deformation. (The same reference also provides a hyperelastic version of the finite strain deformation theory of plasticity for incompressible materials, which is not used here.)

The yield surface is defined via an equivalent von Mises uniaxial stress given by

$$Q = \sqrt{\frac{3}{2}\boldsymbol{S}:\boldsymbol{S}}, \quad \boldsymbol{S} = \boldsymbol{T} - p\boldsymbol{1}, \quad p = \frac{1}{3}\boldsymbol{1}:\boldsymbol{T} \tag{1}$$

where Q is the von Mises equivalent uniaxial stress, $\boldsymbol{T}$ is the Kirchoff stress tensor, $\boldsymbol{S}$ is the deviatoric part of the Kirchhoff stress tensor, $\boldsymbol{1}$ is the unit two-tensor, and a colon (:) is used to indicate the scalar product of 2nd-order tensors[3]. Elastic behaviour occurs within the yield surface, when

$$Q \le Q_0(\lambda) \tag{2}$$

[3] For an orthonormal coordinate system, this scalar product of tensors is simply the sum of the products of each component of the tensors. More generally, for basis vectors $\boldsymbol{g}_j$, the scalar product of two tensors $\boldsymbol{A} = A^{ij}\,\boldsymbol{g}_i\boldsymbol{g}_j$ and $\boldsymbol{B} = Bxs^{ij}\,\boldsymbol{g}_i\boldsymbol{g}_j$ is, $\boldsymbol{A}:\boldsymbol{B} = A^{ij}B_{ij} = A^{ij}g_{ik}g_{jl}B^{kl}$, in which $g_{ij} = \boldsymbol{g}_i \cdot \boldsymbol{g}_j$ are metric coefficients, and summation over repeated indices is implied.

where λ is the equivalent uniaxial logarithmic plastic strain, and the function $Q_0(.)$ may be defined from the results of a uniaxial coupon test[4].

The incremental stress–strain relations for both the flow and deformation theories are best described by using a decomposition of the rate of deformation tensor into a volumetric component, one normal to the yield surface, and one tangent to the yield surface, as follows:

$$\boldsymbol{D} = D_1\mathbf{1} + D_R\boldsymbol{R} + \hat{\boldsymbol{D}} \tag{3}$$

where $\boldsymbol{D}$ is the rate of deformation tensor, $\boldsymbol{R}$ is a tensor normal to the yield surface, given by

$$\boldsymbol{R} = \frac{3}{2Q}\boldsymbol{S} \tag{4}$$

and

$$D_1 = \frac{1}{3}\mathbf{1}{:}\boldsymbol{D}, \qquad D_R = \frac{2}{3}\boldsymbol{R}{:}\boldsymbol{D}, \qquad \hat{\boldsymbol{D}} = \boldsymbol{D} - D_1\mathbf{1} - D_R\boldsymbol{R} \tag{5}$$

The advantage of this decomposition is that the corresponding stress increments for both the flow and deformation theories can be written in a simple form. Specifically, for the flow theory of plasticity, the Jauman rate of the Kirchhoff stress tensor can be written in the form,

$$\overset{\triangledown}{\boldsymbol{T}} = \frac{E}{1-2\nu}D_1\mathbf{1} + 2\,G_T D_R\boldsymbol{R} + 2G\hat{\boldsymbol{D}} \tag{6a}$$

For plastic loading, which occurs when $Q = Q_0(\lambda)$ and $D_R > 0$, and

$$\overset{\triangledown}{\boldsymbol{T}} = \frac{E}{1-2\nu}D_1\mathbf{1} + 2GD_R\boldsymbol{R} + 2G\hat{\boldsymbol{D}} \tag{6b}$$

for elastic unloading, which occurs when $Q < Q_0(\lambda)$ or $D_R < 0$. In Eqs. 6(a, b), E denotes Young's modulus, ν is Poisson's ratio,

$$G = \frac{E}{2(1+\nu)} \tag{7}$$

is the shear modulus, the tangent shear modulus G_T is defined by

$$\frac{1}{G_T} = \frac{3}{H} + \frac{1}{G} \tag{8}$$

[4] It can be shown by integration of the finite deformation constitutive equations in (Needleman and Tvergaard, 1977) for uniaxial loading, that the true equivalent uniaxial stress as defined in Eq. (1) is given by $Q = f(1+\varepsilon_{\text{eng}})$, where f is the nominal stress (force divided by undeformed cross sectional area), and ε_{eng} is the engineering strain (change in length of the test section divided by undeformed length of the test section). The logarithmic plastic strain is given by, $\lambda = \ln(1+\varepsilon_{\text{eng}}) - Q/E$ for a uniaxial tension test, and by $\lambda = -\ln(1+\varepsilon_{\text{eng}}) - Q/E$ for a uniaxial compression test. With these results, a stress-strain relationship between f and ε_{eng} from a uniaxial tension or compression test can readily be transformed into a relationship between Q and λ. The most direct way of defining the function $Q = Q_0(\lambda)$ is by linear interpolation between points where the stresses and strains were recorded in the test. That way one achieves an exact match of the test result for uniaxial loading. Another often-used possibility is the Ramberg–Osgood relationship $\lambda = CQ^n$, in which C and n are constant material parameters defining the strength and strain hardening characteristics of the material.

in which $H = \mathrm{d}Q_0/d\lambda$ is the plastic modulus (slope of the uniaxial true stress–logarithmic plastic strain curve).

For the deformation theory the incremental relations may be written in the form,

$$\overset{\nabla}{\boldsymbol{T}} = \frac{E}{1-2\nu} D_1 \mathbf{1} + 2G_T\, D_R \boldsymbol{R} + 2G_S \hat{\boldsymbol{D}} \tag{9}$$

where G_S is a secant value of the shear modulus, defined in terms of a secant value of the plastic modulus H_S given by

$$\frac{1}{G_S} = \frac{3}{H_S} + \frac{1}{G},\ H_S = \frac{Q_0(\lambda)}{\lambda} \tag{10}$$

It is clear from Eqs. (5), (6a, b) and (9), that the decomposition of the rate of deformation tensor $\boldsymbol{D}$ leads to components that are eigenvectors of the incremental stress–strain relations for all cases. Furthermore, the applicable incremental moduli (eigenvalues) for each of the eigenspaces are as follows:

(i) For the volumetric component of the deformation rate, D_1 $\boldsymbol{1}$, the applicable incremental modulus is always the elastic value $E/(1-2\nu)$.
(ii) For the component normal to the yield surface, D_R $\mathbf{R}$, the applicable incremental modulus is the tangent value $2G_T$ for the deformation theory, and for the flow theory when plastic loading is involved, and it is $2G$ for elastic unloading according to the flow theory. Note that for the deformation theory there is no distinction between elastic unloading and plastic loading. The applicable modulus is $2G_T$ in both cases.
(iii) For the component tangential to the yield surface, $\hat{\boldsymbol{D}}$, the applicable incremental modulus is the elastic value $2G$ for the flow theory (no matter whether the increment involves plastic loading or not), and it is the secant value, $2G_S$ for the deformation theory.

One way to include elastic unloading in the deformation theory of plasticity would be to use the incremental relations of the deformation theory (Eq. (9)) for plastic loading, and the elastic ones (Eq. (6b)) for the elastic unloading. However, this leads to a discontinuity in the incremental stress–strain relations, since the modulus in the direction tangent to the yield surface would jump from $2G_S$, when some plastic loading is involved, to $2G$, when the increment remains within the yield surface. Therefore, a better way needs to be found to include elastic unloading in the context of a deformation theory. Indeed continuity requires that the incremental modulus for the component tangential to the yield surface be the same for loading and unloading.

4. The ICU deformation theory

From the preceding section it is clear in order to formulate a deformation theory including elastic unloading, the incremental modulus for the direction tangent to the yield surface, must be the secant value for both loading and unloading. This results in the following incremental relations,

$$\overset{\nabla}{\boldsymbol{T}} = \frac{E}{1-2\nu} d_1 \mathbf{1} + 2G_T\, D_R \boldsymbol{R} + 2G_S \hat{\boldsymbol{D}}\, g \tag{11a}$$

when $Q = Q_0(\lambda)$ and $D_R > 0$, and

$$\overset{\nabla}{\boldsymbol{T}} = \frac{E}{1-2\nu} d_1 \mathbf{1} + 2G\, D_R \boldsymbol{R} + 2G_S \hat{\boldsymbol{D}} \tag{11b}$$

when $Q < Q_0(\lambda)$ or $D_R < 0$.

The conditions under which Eqs. (11a, b) are applicable might be referred to as "plastic loading" and "elastic unloading", respectively, but this would be misleading, because such "elastic unloading" does involve plastic straining associated with the rotation of the plastic strain tensor, since the secant rather than the elastic value of the material modulus is used for the direction tangent to the yield surface. Therefore, here the phrase "total plastic loading" is used when Eq. (11a) applies, and "pseudo-elastic unloading" when Eq. (11b) applies. Such pseudo elastic unloading is only truly elastic if the stress increment is normal to the yield surface.

The accumulated plastic strain parameter λ for this ICU deformation theory, changes only during total plastic loading, in which case its evolution is defined by the consistency condition $Q = Q_0(\lambda)$. As a result λ is a strictly increasing parameter, as in the flow theory of plasticity.

Plastic deformation within the yield surface is governed by the secant shear modulus G_S. The definition of this quantity in Eqs. (11a, b) applies during total plastic loading, when $Q = Q_0(\lambda)$, but a different definition may be used within the yield surface (where $Q < Q_0(\lambda)$). Indeed to avoid an irregularity in the constitutive relation at zero stress, the condition that $G_S = G$ must be satisfied when $Q = 0$. To achieve this a factor $(Q_0(\lambda)/Q)^m$ is applied to the value of the secant plastic modulus H_S on the yield surface, so that the expression for the secant shear modulus within the yield surface becomes,

$$\frac{1}{G_S} = \frac{3\lambda}{Q_0(\lambda)} \left(\frac{Q}{Q_0(\lambda)} \right)^m + \frac{1}{G} \tag{12}$$

where m is a material parameter that controls the unloading behaviour, or more specifically the amount of plastic deformation within the yield surface. To avoid the singular behaviour at the origin m must be greater than zero. For a large value of m, the first term on the right-hand side of Eq. (12) rapidly becomes very small as the stress state moves away from the yield surface, so that the behaviour then becomes essentially elastic, and significant plastic deformations can occur only very close to the yield surface. On the other hand, for smaller m, plasticity effects can still be significant at a larger distance from the yield surface. A reasonable value is $m = 10$. In any case, initially, before any plastic deformation has taken place, $\lambda = 0$, so that the behaviour then is fully elastic at all points within the initial yield surface no matter what the value of m. Also, if no elastic unloading occurs, then the results will be independent of the material parameter m.

The implementation of this ICU deformation theory of plasticity can proceed in exactly the same way as that of the flow theory of plasticity using an elastic predictor – radial return type algorithm, except that in this case it becomes a pseudo-elastic predictor–radial return algorithm, with the pseudo-elastic predictor being calculated based on elastic incremental moduli for the direction normal to the yield surface, but secant incremental moduli for the direction tangent to the yield surface. Details are given in Appendix A.

5. Example: axisymmetric buckling of a cylinder under axial compression

The problem of plastic buckling of cylinders under axial stresses has been dealt with quite extensively in the literature (Batterman, 1965; Bushnell, 1982; Tvergaard, 1983; Giezen, 1988; Teng, 1994; Mikkelsen, 1995; Blachut et al., 1996; Mikkelsen, 1996). Indeed, it is known that axisymmetry-breaking bifurcations and/or secondary bifurcations can occur (Tvergaard, 1983; Mikkelsen, 1995). However, here the intent is only to illustrate differences between the flow and ICU deformation theory, and the

corresponding imperfection sensitivity in each case. Therefore, attention is focused only on the simplest case of axisymmetric behaviour. Even though axisymmetry-breaking buckling modes are ignored here, the example still serves its intended illustrative purpose.

The properties of the cylinder are taken to be: $D/t = 20$ for the outer-diameter-to-thickness ratio, $\nu = 0.3$ for Poisson's ratio, and a stress–strain curve defined by the Ramberg–Osgood type relation,

$$\lambda = \frac{3}{7}\frac{Q}{E}\left(\frac{Q}{Q_{\text{ref}}}\right)^{n-1} \tag{13}$$

where

λ is the equivalent uniaxial logarithmic plastic strain, as defined previously,
E is Young's modulus, taken as $E = 207$ GPa,
Q is the true stress, as defined previously,
n is a material parameter, taken as $n = 7.5$, and
Q_{ref} is a yield stress parameter taken as $Q_{\text{ref}} = 290.72$ MPa.

These material parameters given imply a stress and strain at ultimate that is typical of an API 5L grade X65 carbon steel pipe, but the Ramberg–Osgood stress–strain curve used here does not include the plateau that is often observed on for seamless carbon steel pipes.

For the perfect tube, a finite strain version of Batterman's result (Peek, 1999) yields a bifurcation strain of 2.84%, using the deformation theory, as described here. (The bifurcation strains are the same for the ICU and true deformation theories.) This analytical solution based on thin shell theory also provides a critical half wavelength for the wrinkles of 5.55 t, where t is the wall thickness. The bifurcation analysis is also performed by modelling a section of the cylinder with axisymmetric finite elements. The length of the section modelled was taken as the critical half wavelength of the wrinkles from the analytical solution, and symmetry boundary conditions were used at each end, since these are the conditions that are satisfied by the analytical solution. The mesh consists of 7×100 four-noded axisymmetric elements with reduced integration and hourglass control according to the approach in (Belytschko and Ong, 1984). On this basis it was found that the axial shortening at bifurcation was 2.68%. This is about 6% lower than that from the analytical solution, which is not unreasonable in view of (i) discretisation errors arising from using seven elements across the thickness[5], and (ii) errors introduced by the thin shell theory approximation by which shear deformations are neglected.

The bifurcation strains could also be computed based on the flow theory, but this typically gives very high bifurcation strains. Indeed, the finite element solution based on the flow theory was carried to an axial shortening of over 50% without any bifurcation being found[6]. (The bifurcation strains for the finite deformation flow theory are even larger than those for the corresponding small strain theory shown in Fig. 1).

The finite element analysis is also performed for pipes with a geometric imperfection in the same shape as the bifurcation buckling mode. This involves a sinusoidal variation of radial displacements along the length of the pipe with the same half wavelength of 5.55 t, obtained from the analytical finite-strain wrinkling solution. The size of the imperfection is described by an amplitude parameter a, which

[5] Due to the reduced integration of the elements used, with seven elements across the thickness, the apparent shell section flexural rigidity that is 2% below the exact value.

[6] The bifurcation point is found by first performing the analysis with additional constraints imposed to prevent the development of wrinkling type deformations, and then releasing these constraints to perform a stability check on the tangent stiffness matrix of the released system. Without these constrains it was found (at least for the flow theory) that small numerical truncation errors tend to grow close to exponentially until finally limit point behaviour rather than bifurcation behaviour is encountered.

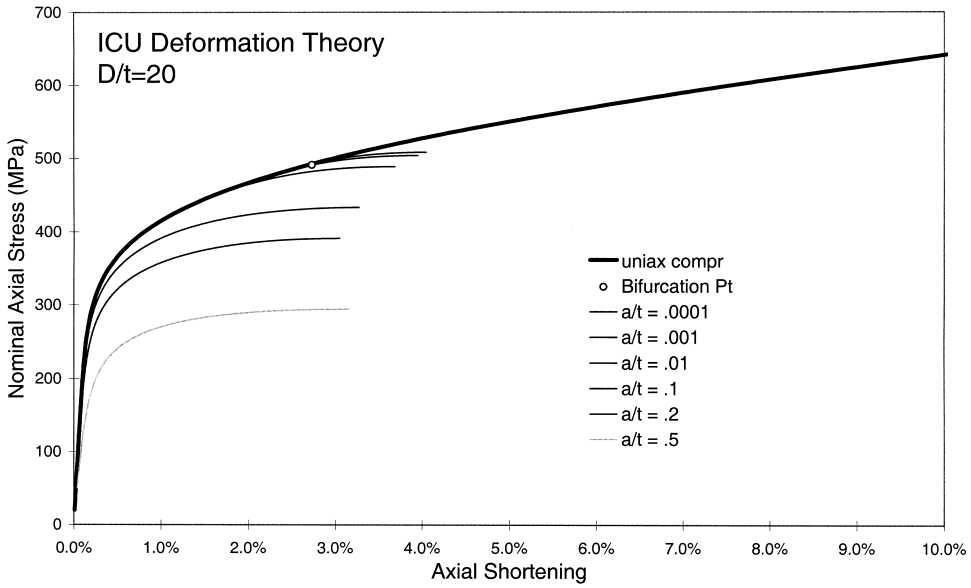

Fig. 3. Load-axial shortening relations for pipes with sinusoidal imperfections under axial compression from the ICU deformation theory of plasticity.

represents the maximum change in radius from the mean radius. (Thus the difference between maximum and minimum diameter is 4*a*.) Typical axial load-shortening relations for different sizes of the imperfection are shown in Fig. 3 for the ICU deformation theory, and in Fig. 4 for the flow theory. Therein the axial load is expressed as a nominal stress, defined as the axial force divided by the undeformed cross-sectional area.

In Figs. 3 and 4, the curves labelled "Uniax Compr" are the principal solution. That is they represent the load-shortening curve for the perfect cylinder when no buckling deformations are allowed to develop.

For the ICU deformation theory (Fig. 3), the solutions for the imperfect system are seen to converge as the imperfection becomes very small. They converge to the bifurcated solution for the perfect system. This bifurcated solution involves initially increasing load. Such behaviour is associated with elastic unloading, and coincides with the prediction from Hill's general theory of bifurcation in the plastic range (Hutchinson, 1974). Indeed, Hill's general bifurcation theory is directly applicable to the ICU deformation theory, just as it is to the flow theory, since in both cases the incremental stress–strain relation is bilinear and continuous.

The increase in load beyond the bifurcation point is not observed for a true deformation theory of plasticity that does not represent unloading. Such a true deformation theory is in essence a nonlinear elastic material model[7]. For it the behaviour in the vicinity of the bifurcation point is that of an imperfection sensitive elastic structure with a symmetric bifurcation point (Koiter, 1945; Budiansky,

[7] The "true" deformation theory of plasticity used here employs the same incremental moduli as the ICU deformation theory moduli for plastic loading irrespective of whether the equivalent von Mises stress is increasing or decreasing. As such this "true" deformation theory strictly represents a nonlinear material only in the small strain range. In the finite strain range when changes in the principal axes of loading are involved this "true" deformation theory represents a hypoelastic rather than a hyperelastic material model.

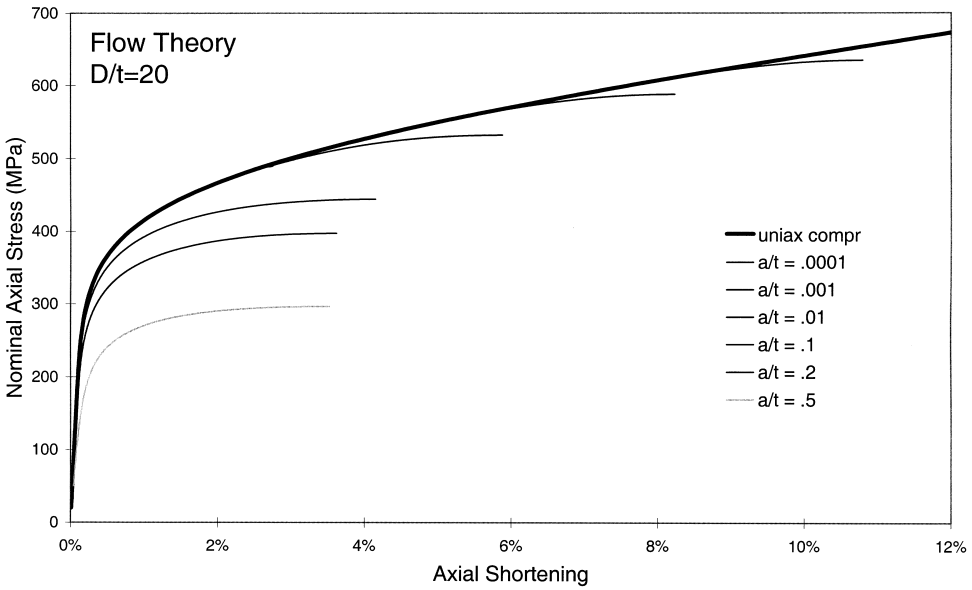

Fig. 4. Load-axial shortening relations for pipes with sinusoidal imperfections under axial compression from the flow theory of plasticity.

1974; Triantafyllidis and Peek, 1992). As such, the load on the bifurcated branch starts to drop immediately, and the load-carrying capacity of the imperfect structure can never exceed the bifurcation load. This is illustrated in Fig. 5, where the load-shortening relations for the ICU and true deformation

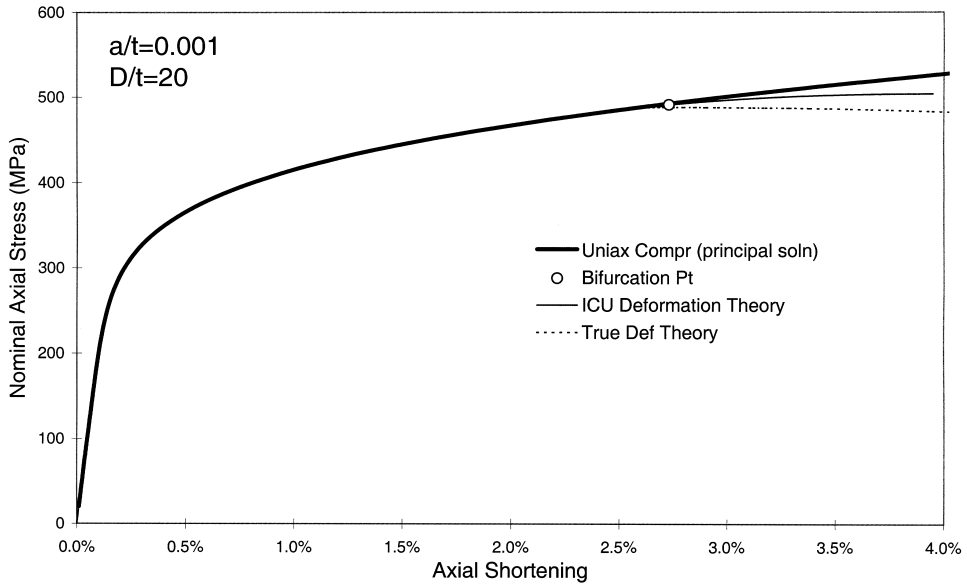

Fig. 5. Comparison of load-axial shortening relations for ICU and true deformation theories of plasticity in the presence of a small ($a/t = 0.001$) imperfection.

theories are compared for the case when a small imperfection is involved, so that the solutions are quite close to the bifurcated solution for the perfect system. The observed change in slope of the load-shortening curve at the transition from the principal to the bifurcated solution branch is characteristic of a symmetric bifurcation in an elastic system (Koiter, 1945; Budiansky, 1974; Triantafyllidis and Peek, 1992). This change in slope does not occur for the case of plastic buckling where the direction of the bifurcated solution is determined by a neutral loading condition (Hutchinson, 1974).

In contrast to the deformation theories, for the flow theory, no convergence of the solutions as the imperfections become vanishingly small is observed up to imperfections as small as $a/t = 0.0001$ (Fig. 4). Instead the axial strain at which the solution for the imperfect system veers away from the principal solution keeps on increasing by a roughly equal amount each time the size of the imperfection is decreased by a factor of 10. This behaviour can be seen more clearly on a logarithmic plot showing the growth of the imperfections for the flow theory (Fig. 6). It shows that very small imperfections grow roughly exponentially with increasing axial shortening. When one considers that the bifurcation strain is over 50% for the flow theory (as opposed to 2.7% for the deformation theory), it is not surprising that no convergence to the bifurcated solution for the perfect cylinder is observed. An imperfection sufficiently small to reach a state close to the bifurcation point would have to be very small indeed. Specifically by roughly extrapolating from Fig. 6 the initial imperfection would have to be as small as $a/t = 10^{-15}$ to be able to reach an axial shortening of around 50% without buckling.

The limit point (where the maximum load is reached) is of particular interest, not only because it provides the load-carrying capacity of the tube, but also because it describes the point beyond which localisation of deformations will occur, if the pipe tested is several half wavelengths long. The curves in Figs. 3 and 4 all stop at the limit point. The load and axial shortening at this point are also plotted in Figs. 7 and 8, respectively, for all three plasticity theories considered. The level of the bifurcation stress and strain are also indicated in Figs. 7 and 8 by dashed lines. As expected (Koiter, 1945; Budiansky, 1974; Hutchinson, 1974; Triantafyllidis and Peek, 1992) convergence of the limit point for the imperfect

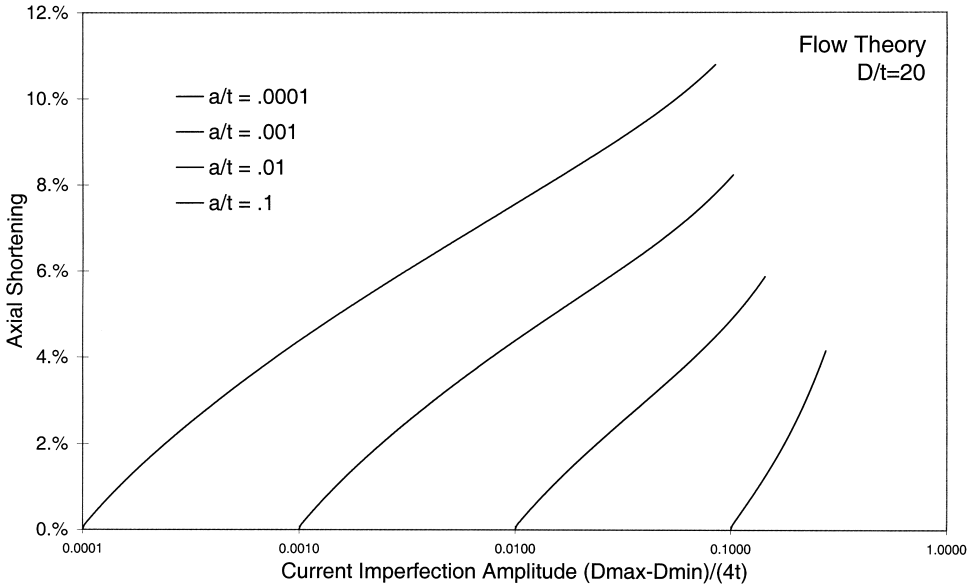

Fig. 6. Growth of imperfections of various sizes from flow theory of plasticity during axial loading of a cylinder.

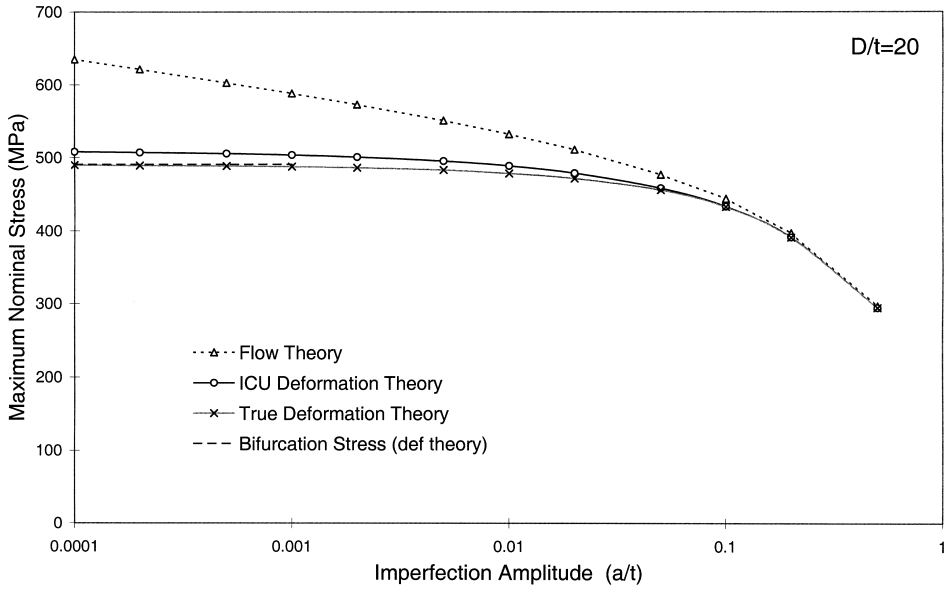

Fig. 7. Effect of imperfection amplitude on load-carrying capacity (nominal stress at limit point) for a $D/t = 20$ pipe.

system to the bifurcation point as the imperfection becomes vanishingly small only occurs for the true deformation theory. For imperfections exceeding about 10% of the wall thickness the flow and deformation theories yield much the same results. Also there is no unloading for such larger imperfections,

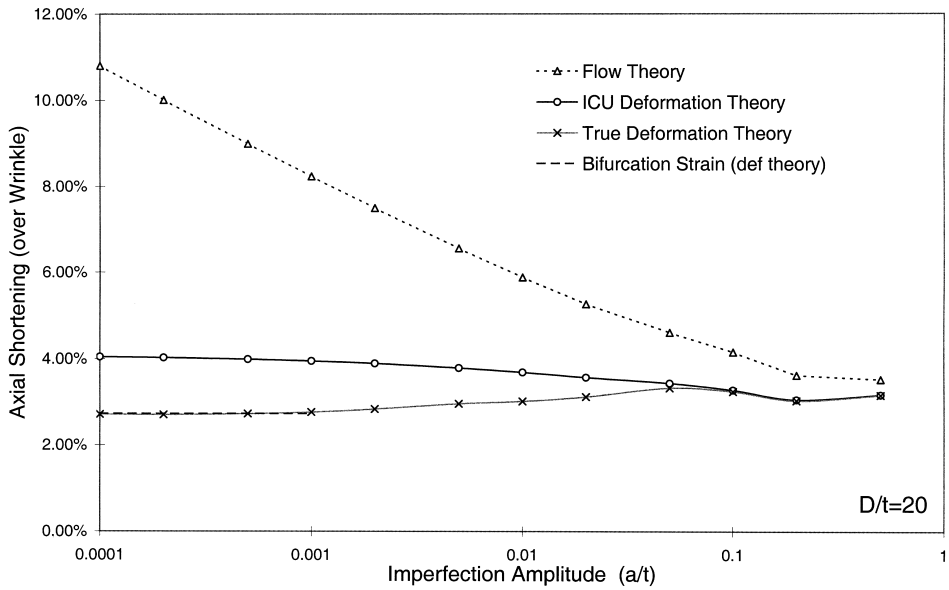

Fig. 8. Effect of imperfection amplitude on axial shortening at limit point for a pipe with $D/t = 20$ under axial compression according to flow and ICU deformation theory of plasticity.

Table 1
Test parameters for wrinkling tests on pressurised 12-in. carbon steel pipes

Specimen name	Temperature (°C)	Internal pressure (psi)	Maximum applied axial shortening (%)
NTNP	Room	No pressure	5.89
HTNP	160	No pressure	6.26
HTLP	160	3410	6.06
HTHP	160	7120	6.12

so the difference between the true and ICU deformation theories disappears completely. For smaller imperfections, however, the differences become significant, and for the flow theory the limit point stress and strain continue to grow approximately linearly with the logarithm of the initial imperfection size.

6. Comparison to test results

In addition to comparing buckling predictions for the imperfect system with the flow and deformation theories, it is essential to see where the experimental results lie in relation to these predictions. For this purpose a set of test results is needed for which the imperfections are sufficiently well known, so that they can be included in the finite element model. Such a set of results was recently obtained by Shell UK. A total of four pipes of 12-in. nominal diameter were tested under axial load and internal pressure. The names of the specimen and test parameters are shown in Table 1. All pipes satisfied the API 5L grade X65 specification, and had an initial wall thickness of about 34 mm. However, the specimen were machined down to about 27 mm wall thickness over a 650 mm-long test section, giving them an outer-diameter-to-thickness ratio of about $D/t = 10$ over the test section. The transition from the test section to the full wall thickness occurs over a length of about 75 mm. This transition in wall thickness acts as

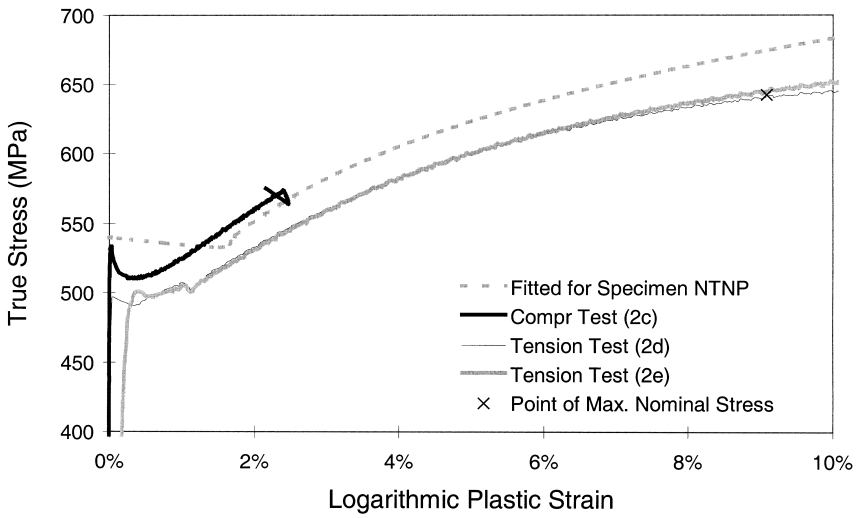

Fig. 9. Stress–strain curves for specimen NTNP (tested at room temperature). The "fitted" curve is the one used in the finite element analyses. Tension test results are from round bar specimen, and the compression test is performed on a 25 mm diameter and 40 mm long solid cylinder.

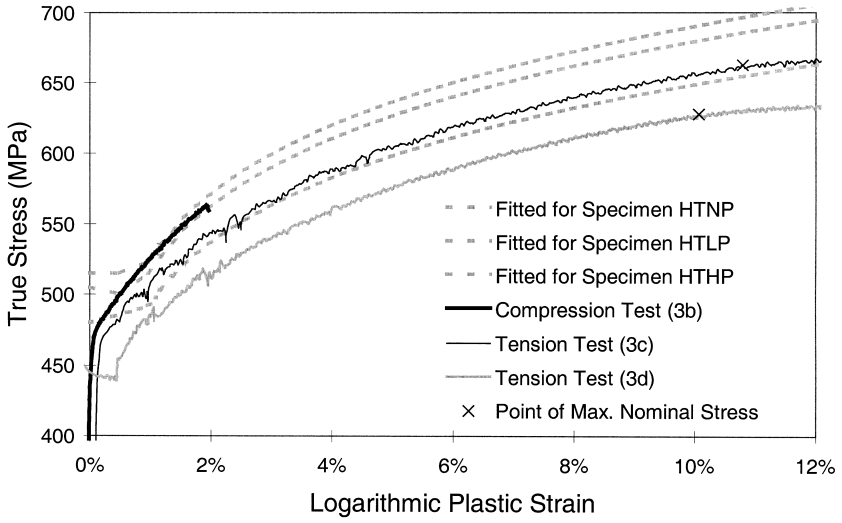

Fig. 10. Stress–strain curves for the specimen tested at elevated temperature. The stress–strain tests were performed at the same temperature of 160°C as the wrinkling test on the specimen. The "fitted" curves are those used in the finite element analysis. For these the yield stress is adjusted to match the observed yielding load of the specimen during the wrinkling test.

the imperfection that induces wrinkling type deformations. The wall thickness increases by a factor of about 1.3 over the transition.

Measured stress–strain curves are shown in Figs. 9 and 10, for coupon tests performed at room temperature and at 160°C, respectively. These figures also show the stress–strain curves used in the finite element analyses of the specimen as grey dotted lines, which are labelled "fitted" curves. Indeed in view of the point-to-point variabilities in yield stress observed in the pipe, the "fitted" curves were scaled to match the observed yield stress during the wrinkling tests. The strain hardening portion of the fitted tests is represented by a Ramberg–Osgood type curve (Eq. (13)), with an exponent of $n = 7.5$ for the tests at room temperature and $n = 8.5$ for the tests at elevated temperature. It is apparent from Figs. 9 and 10, that these values of the exponent provide a reasonable fit to the measured stress–strain curves in range from 2% to 8% strain. (This is true even though the fitted curves imply a strain at ultimate of $1/n$, which exceeds the observed strains of about 10%, as indicated in Figs. 9 and 10.)

All tests proceeded to about 6% axial shortening with increasing axial load, at which point the test was stopped, the specimen unloaded, and the residual plastic deformations measured. Exactly the same procedure was simulated in the finite element analysis, using axisymmetric finite elements and matching the actual (measured) geometry of each of the test specimen. Indeed, to make the results comparable, the axial shortening during the finite element analysis was monitored over the same gauge length that was used in the tests[8].

The comparisons of the final calculated and measured[9] residual plastic deformations are shown in

[8] This axial shortening was measured over an 800 mm-long gauge length, which includes the 650 mm-long test section. This means that the axial shortening over the test section can be expected to be somewhat higher, but not by more than a factor of 1.2, which would imply a maximum axial shortening of about 7.2% over the test section.

[9] The measured radial deflection is determined from the growth in diameter in various azimuthal directions, and at each side of the plane of symmetry. That way the maximum, minimum and average values plotted for each value of the axial coordinate were determined.

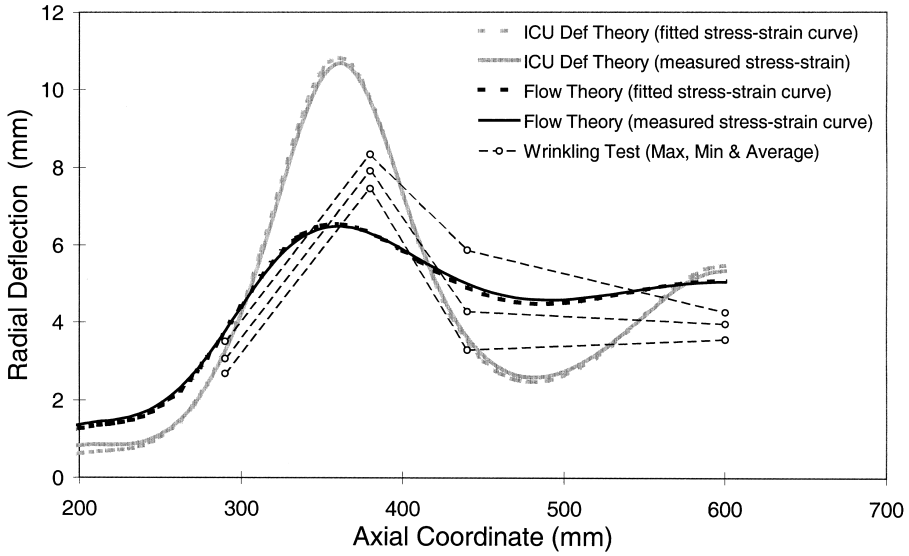

Fig. 12. Comparison of the calculated and measured post-test radial deflections as a function of the axial coordinate for specimen HTNP. Test was performed at a temperature of 160°C, without internal pressure. The axial coordinate has its origin at the end-cap. Only half of the specimen is drawn, but maxima and minima include readings from both sides.

Figs. 11–14. Therein the axial coordinate takes a value of $x = 600$ mm at the centre of the test section, which is taken as a plane of symmetry for the analysis. The transition in wall thickness occurs between $x = 200$ and $x = 275$ mm. Clearly wrinkling-type deformations are induced by the change in wall

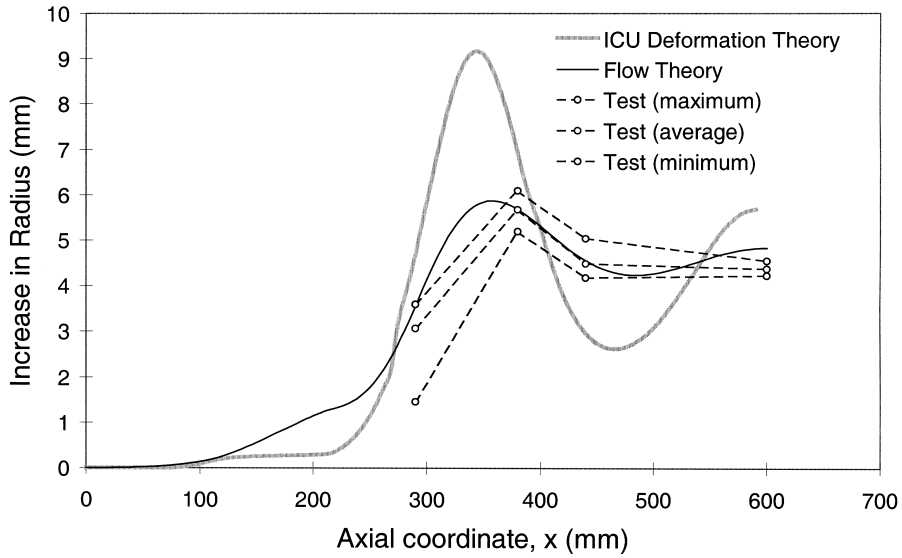

Fig. 11. Comparison of the calculated and measured post-test radial deflection as a function of the axial coordinate for specimen NTNP. Test was performed at room temperature without internal pressure. The axial coordinate has its origin at the end-cap. Only half of the specimen is covered, but maxima and minima include test readings from both sides.

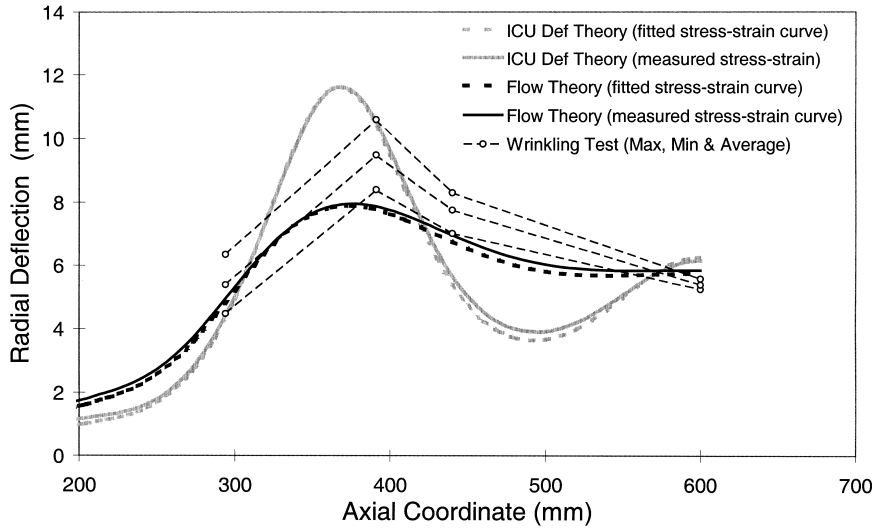

Fig. 13. Comparison of calculated and measured post-test radial deflection as a function of the axial coordinate for specimen HTLP. Test was performed at a temperature of 160°C with an internal pressure of 3410 psi. The axial coordinate has its origin at the end-cap. Only half of the specimen is drawn, but maxima and minima include readings from both sides.

thickness. This degree of wrinkling type deformation is overpredicted by the ICU deformation theory in all cases, but it is underpredicted by the flow theory for specimen HTNP and HTLP, whereas for the other specimen (NTNP and HTHP), the flow theory predicts about the correct amount of wrinkling

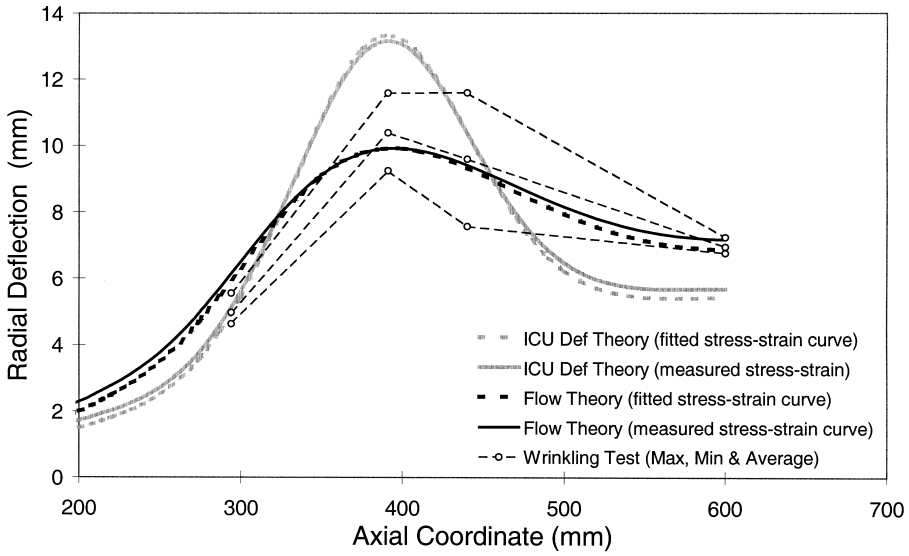

Fig. 14. Comparison of calculated and measured post-test radial deflection as a function of the axial coordinate for specimen HTHP. Test was performed at a temperature of 160°C with an internal pressure of 7120 psi. The axial coordinate has its origin at the end-cap. Only half of the specimen is drawn, but maxima & minima include readings from both sides.

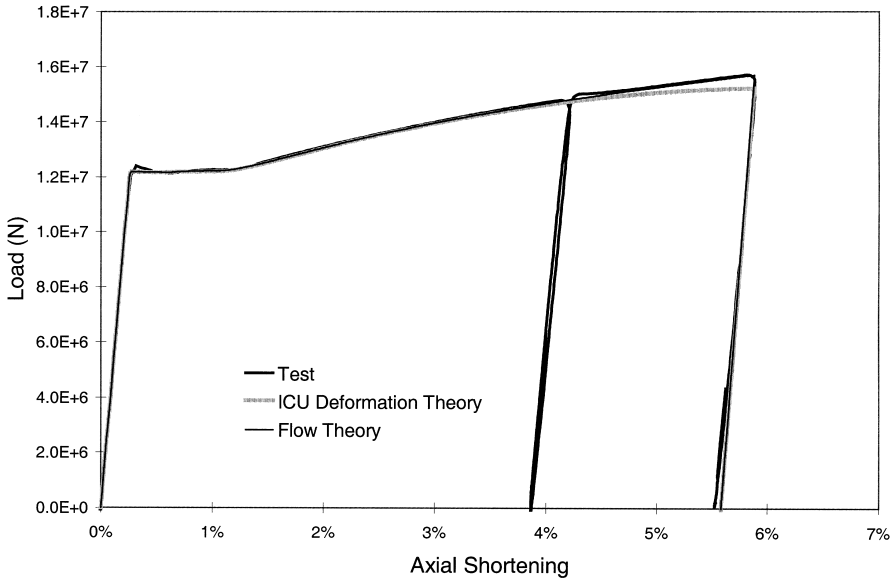

Fig. 15. Axial load-shortening relations over 800 mm-long gauge length for specimen NTNP.

type deformation. On the whole the flow theory provides closer predictions of the wrinkling type deformations for these tests.

Load-shortening relations for the test and the analyses are compared in Figs. 15 and 16. In both cases the test results, and those from the flow and ICU deformation theories are virtually indistinguishable up

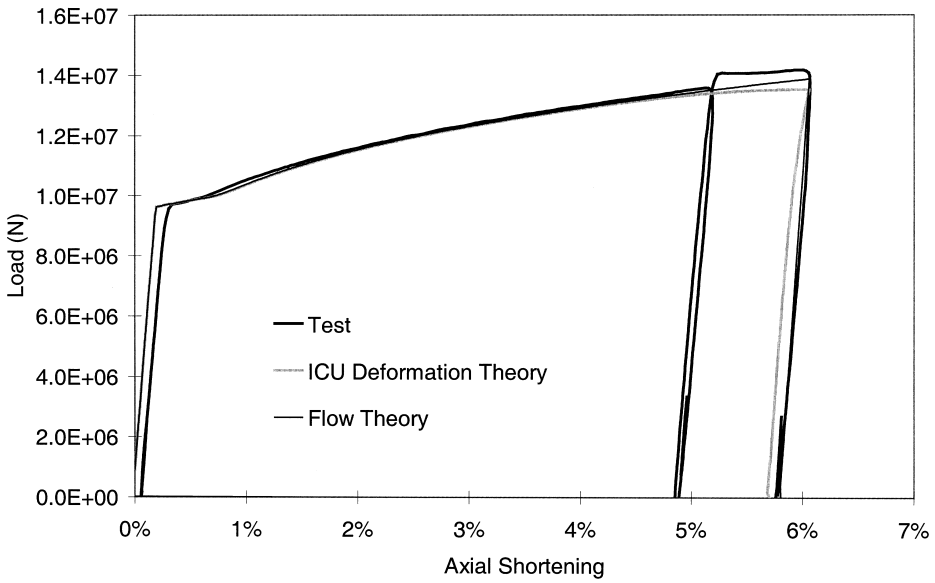

Fig. 16. Axial load-shortening relations over 800 mm-long gauge length for specimen HTHP.

to about 4% axial shortening. Beyond that the test and flow theory results are still in excellent agreement, but the ICU deformation theory yields somewhat lower loads. This is consistent with the larger wrinkling type deformations for the ICU deformation theory.

The very close agreement between theory and test results in Figs. 15 and 16 was achieved by to some extent scaling of the stress-plastic strain curves. Nevertheless, the ''fitted'' stress–strain curves thus obtained fall quite close to the measured stress–strain data (see Figs. 9 and 10). They fall especially close to the results of the compression test for the case of the unpressurised specimen (NTNP and HTNP). Also the Ramberg–Osgood exponent for the fitted stress–strain curves was determined from the stress–strain data. Therefore, the matching of load-shortening curves in Figs. 15 and 16 is not entirely fabricated. The prediction of the shapes of the curves is good, even when it is based only on the stress–strain data from axial coupon tension tests. (Unfortunately the compression tests could not be carried to strains above 2% because of lateral buckling of the specimen. These tests were carried out on solid cylindrical specimen with a length to diameter ratio of about 1.6. The axial strains were measured at four evenly spaced locations around the circumference at the middle of the specimen, so that it could be verified that essentially no bending of the specimen occurred during the tests.)

The effect of pressurisation on the fitted stress–strain curves can be seen in Fig. 10 by comparing the fitted curves for specimen HTNP, HTLP, and HTHP. The higher the internal pressure, the lower the fitted curve. Specifically the drop of the fitted stress–strain curve below that for the unpressurised case (HTNP) is about 10 MPa for the low internal pressure (HTLP), and 50 MPa for the high pressure case (HTHP). Those differences suggest that the theory based on the von Mises yield criterion, somewhat underestimates the reduction in axial compressive stress at yield due to the internal pressure. Indeed, the observed behaviour lies in between that for the von Mises and Tresca yield criteria, with the weighting factors being about 80% von Mises and 20% Tresca for HTLP, and 50%/50% for HTHP (based on the assumption that these observed differences in the fitted stress–strain curves are entirely due to the shape of the yield surface).

The effect of unloading and reloading on the test results is also of some interest. This occurred at about 5% axial shortening (see Figs. 15 and 16). When the specimen was reloaded, its yield strength seems to have increased slightly beyond the maximum load the specimen had experienced previously. This is probably a result of a change in material properties due to diffusion of solution elements such as nitrogen within the steel. Such elements are known to diffuse into interstitial locations created by the dislocations. That way they inhibit the further propagation of the dislocation, giving rise to the observed increase in strength. However, once further plastic deformation causes the dislocation to move away from the blocking interstitial atom, the behaviour of the steel is back to what it would have been without the unloading and reloading event. At higher temperature the diffusion of the interstitial elements is faster, leading to a more pronounced effect. This temperature dependence of the effect is also observed when comparing Figs. 15 and 16.

7. Conclusions

A simple way to include unloading in a deformation theory of plasticity is given, by which continuity of the incremental stress–strain relations is maintained. This deformation theory is, therefore, referred to as the ICU deformation theory, since the material model is Incrementally Continuous and includes Unloading. This incremental continuity could only be achieved by allowing plastic deformations within the yield surface. (Such plastic deformations are associated with rotation of the plastic strain tensor in line with rotations of the deviatoric stress tensor). A parameter m is introduced that governs the extent to which such plastic deformations are possible within the yield surface. (For larger m the possibility of

plastic deformation decreases more rapidly as the stress state moves towards the interior of the yield surface.) The resulting theory has the following characteristics:

1. For proportional loading, unloading and reverse loading (i.e. when the stress state is always on the same straight line through the origin in stress space), it coincides with the flow theory of plasticity. This means that for problems such as the Euler buckling of a column (where the stresses act always along the same axial direction, but may change from tension to compression) the new theory will give the same results as the flow theory, for bifurcation buckling as well as postbuckling and imperfection sensitivity. (In contrast the standard deformation theory is not suitable for such postbuckling analysis, since elastic unloading does already occur in the postbuckling regime before the maximum load carrying capacity is reached.)
2. For calculations of incipient buckling (or necking) by bifurcation of the solution path, the ICU deformation theory gives the same results as the standard deformation theory, which is known to be generally in better agreement with the experimental data.
3. As for the flow theory of plasticity, the ICU deformation theory is incrementally continuous and bilinear. As a result no extra difficulties are expected in the numerical solution procedures. Furthermore Hill's general theory of bifurcation remains applicable, and can be used to determine the direction of the bifurcated solution branches that emanate at a bifurcation point.

Another advantage of the approach is that it can be implemented with minimal changes to an existing elastic predictor–radial return algorithm for the J2 flow theory of plasticity. Indeed, only the calculation of the elastic predictor is changed.

Caution must be exerted when the prebifurcation behaviour involves non-proportional loading (such as for the puckering instabilities in the forming of a hemispherical cup (Triantafyllidis, 1985), or bending of pipes, where the prebifurcation nonlinearity arises due to ovalisation of the cross-section), since in absence of unloading the ICU deformation theory still does not include any path dependent effects.

The approach is particularly useful in design situations where the exact manner in which the yield surface will evolve is not known, but one would like to obtain a lower bound to the load or deformation capacity of the system in addition to an upper bound from the J2 flow theory.

Acknowledgements

This work has been performed as part of the Evolutionary Technology Development Program at Shell International Exploration and Production, B.V., with sponsorship from a number of Shell Operating Units, but mainly from Shell UK Exploration and Production. The wrinkling tests were sponsored by the ETAP project, and performed by Albert Holt of Mitsui Babcock. The finite element calculations used in the comparisons with the test results were performed by A. de Jonge. Finally two anonymous reviewers quite carefully read the manuscript providing very constructive comments.

Appendix A. Implementation of the ICU deformation theory

The incremental stress–strain relations of the flow theory of plasticity can be written as

$$\overset{\nabla}{\boldsymbol{T}} = \boldsymbol{L}:\left(\boldsymbol{D} - \dot{\lambda}\boldsymbol{R}\right), \boldsymbol{L} = 2G\left(\boldsymbol{I} + \frac{\nu}{1-2\nu}\boldsymbol{1}\boldsymbol{1}\right) \tag{A1}$$

in which $\boldsymbol{I}$xs is the fourth order identity tensor, and λ is defined by the requirements that either

$$\dot{\lambda} > 0 \text{ and } Q = Q_0(\lambda) \tag{A2}$$

for plastic loading, or

$$\dot{\lambda} = 0 \text{ and } Q \leq Q_0(\lambda) \tag{A3}$$

for elastic behaviour. All other quantities in Eqs. (A1)–(A3) are defined in the main body of this paper.

Eqs. (A1)–(A3) also apply for the ICU deformation theory, except that in this case the elastic incremental stiffness tensor $\boldsymbol{L}$ is replaced by a tensor

$$\boldsymbol{L}_{es} = \frac{1}{3}\left(\frac{E}{1-2\nu} - 2G_S\right)\mathbf{11} + 2G_S\boldsymbol{I} + \frac{4}{3}(G - G_S)\boldsymbol{RR} \tag{A4}$$

which represents elastic moduli normal to the yield surface but secant moduli tangent to the yield surface. Thus, ICU deformation theory is defined by incremental relation

$$\overset{\nabla}{\boldsymbol{T}} = \boldsymbol{L}_{\mathbf{es}}:(\boldsymbol{D} - \dot{\lambda}\boldsymbol{R}) \tag{A5}$$

together with Eqs. (A2) and (A3) providing the additional conditions for plastic loading and unloading, respectively.

To obtain the corresponding relations in component form, the Kirchhoff stress tensor, and the rate of deformation tensor are written in terms of convected covariant basis vectors $\boldsymbol{g}_i$ and their contravariant counterparts $\boldsymbol{g}^i$ in the form,

$$\boldsymbol{T} = T^{ij}\boldsymbol{g}_i\boldsymbol{g}_j, \qquad \boldsymbol{D} = D_{kl}\boldsymbol{g}^k\boldsymbol{g}^l \tag{A6}$$

The Jauman rate of the tensor $\mathbf{T}$ can then be written as

$$\overset{\nabla}{\boldsymbol{T}} = \overset{\circ}{\boldsymbol{T}} - \boldsymbol{D}\cdot\boldsymbol{T} - \boldsymbol{T}.\boldsymbol{D} \tag{A7}$$

in which

$$\overset{\circ}{\boldsymbol{T}} = \dot{T}^{ij}\boldsymbol{g}_i\boldsymbol{g}_j \tag{A8}$$

is the convective rate of the Kirchhoff stress tensor $\boldsymbol{T}$. Using these results to write the incremental stress–strain relations of the ICU deformation theory in component form yields

$$\dot{T}^{ij} = \left(L_{\text{es}}^{ijkl} - T^{ik}g^{jl} - T^{jk}g^{il}\right)D_{kl} - 2G\dot{\lambda}R^{ij} \tag{A9}$$

in which a dot placed above any quantity denotes differentiation with respect to time, and

$$L_{\text{es}}^{ijkl} = \frac{1}{3}\left(\frac{E}{1-2\nu} - 2G_S\right)g^{ij}g^{kl} + 2G_Sg^{ik}g^{jl} + \frac{4}{3}(G - G_S)R^{ij}R^{kl} \tag{A10}$$

$$R^{ij} = \frac{3}{2Q}S^{ij}, \qquad S^{ij} = T^{ij} - pg^{ij}, \qquad p = \frac{1}{3}T^{kl}g_{lk}, \qquad Q = \sqrt{\frac{3}{2}S^{ij}g_{ik}g_{jl}S^{kl}} \tag{A11}$$

$$g_{ij} = \boldsymbol{g_i}.\boldsymbol{gxs_j}, \qquad \left[g^{ij}\right] = \left[g_{ij}\right]^{-1} \tag{A12}$$

Finally the components of the rate of deformation tensor $\boldsymbol{D} = D_{kl}\boldsymbol{g}^k\boldsymbol{g}^l$ can be written as

$$D_{kl} = \dot{E}_{kl} = \frac{1}{2}\dot{g}_{kl} \tag{A13}$$

in which E_{kl} are the components of the Green–Lagrange strain tensor.

To obtain relations that can be applied for a finite increment, the following approximations are made:

1. the time derivatives appearing in Eq. (A9) are replaced by the change in the corresponding quantity over the increment;
2. the metric coefficients and g_{ij} and g^{ij} are always evaluated at the end of the increment, but the components of the stress tensor and the moduli are evaluated at the beginning of the increment, except that
3. the tensor components R^{ij} in Eq. (A9) are evaluated at the end of the increment.

In this manner one obtains,

$$[T^{ij}]_1 = T^{ij}_{\text{es}} - 2G[R^{ij}]_1\Delta\lambda \tag{A14}$$

where

$$T^{ij}_{\text{es}} = [T^{ij}]_0 + \left[L^{ijkl}_{\text{es}} - T^{ik}g^{jl} - T^{jk}g^{il}\right]_{0\&1}\Delta E_{kl} \tag{A15}$$

is an elastic predictor value for the stresses, and for any quantity or expression (.), $[(.)]_0$ denotes the value at the beginning of the increment, $[(.)]_1$ denotes the value at the end of the increment,

$$\Delta(\cdot) = \left[(\cdot)\right]_1 - \left[(\cdot)\right]_0 \tag{A16}$$

denotes the change in value over the increment, and $[(.)]_{0\ \&\ 1}$ indicates that the stresses and material moduli enclosed in the brackets are to be evaluated at the beginning of the increment, but the metric coefficients are to be evaluated at the end of the increment.

It follows from Eq. (A14) that radial return applies, and furthermore, for plastic loading the increment in accumulated plastic strain λ is determined from,

$$Q_0\left([\lambda]_0 + \Delta\lambda\right) + 3G\Delta\lambda = Q^{\text{es}} \tag{A17}$$

in which

$$Q^{\text{es}} = \sqrt{\frac{3}{2}S^{ij}_{\text{es}}[g_{ik}g_{jl}]_1 S^{kl}_{\text{es}}} \tag{A18}$$

$$S^{ij}_{\text{es}} = T^{ij}_{\text{es}} - p^{\text{es}}g^{ij},\ p^{\text{es}} = \frac{1}{3}T^{kl}_{\text{es}}g_{lk} \tag{A19}$$

Finally, having obtained the plastic strain increment, $\Delta\lambda$, the stress increment is given by

$$[T^{ij}]_1 = T^{ij}_{\text{es}} - \frac{3G\Delta\lambda}{Q^{\text{es}}}S^{ij}_{\text{es}} \tag{A20}$$

Thus, the only difference between the implementation of this ICU deformation theory of plasticity and a conventional flow theory lies in that the elastic predictor value of the stress is calculated using incremental moduli $\boldsymbol{L}_{\text{es}}$ rather than $\mathbf{L}$.

In summary the procedure to be followed for every increment is as follows:

1. Calculate the elastic predictor stresses from Eq. (A15).
2. Calculate Q^{es} from Eqs. (A18) and (A19). If $Q^{\mathrm{es}} > Q_0([\lambda]_0)$ solve Eq. (A17) for the plastic strain increment $\Delta\lambda$ (as is done for the flow theory). Otherwise $\Delta\lambda = 0$.
3. Compute the new stress state from Eq. (A20).

By virtue of the manner in which the time discretisation is constructed here, the accumulated error should be of the order of the size of the increment, and will therefore become vanishingly small as the size of the increments is decreased to zero. This convergence of the time discretisation has also been verified numerically for one of the examples of Section 5.

In order to calculate the tangent stiffness matrix, the incremental relations written in the form

$$\dot{T}^{ij} = L_{\mathrm{ts}}^{ijkl}\dot{E}_{kl} \text{ (for plastic loading)} \tag{A21a}$$

$$= L_{\mathrm{es}}^{ijkl}\dot{E}_{kl} \text{ (for elastic unloading)} \tag{A21b}$$

where L_{es}^{ijkl} is given in Eq. (A10), and

$$L_{\mathrm{ts}}^{ijkl} = L_{\mathrm{es}}^{ijkl} - \frac{4G^{2}}{H+3G}R^{ij}R^{kl} = \frac{1}{3}\left(\frac{E}{1-2\nu} - 2G_S\right)g^{ij}g^{kl} + 2G_S g^{ik}g^{jl} + \frac{4}{3}(G_{\mathrm{T}} - G_S)R^{ij}R^{kl} \tag{A22}$$

It is known that using consistent incremental moduli can lead to faster convergence of the Newton iteration type solution schemes used in the finite element calculations. However, for the algorithm described here the consistent stiffness matrix is not symmetric. In view of this, and of the effort involved in constructing expressions for the consistent stiffnesses, the symmetric incremental stiffness matrix defined by Eqs. (A21a, b), rather than the consistent stiffnesses are used in the finite element computations. For sufficiently small steps this still leads to rapid convergence of the Newton iterations at each increment. (Note that although use of the consistent matrices can result in more rapid convergence of the Newton iterations, it does not improve the accuracy of the results, which are still dominated by discretisation errors in time and in space.)

References

Batterman, S.C., 1965. Plastic buckling of axially compressed cylindrical shells. AIAA Journal 3 (2), 316–325.

Belytschko, T., Ong, J.S.J., 1984. Hourglass control in linear and nonlinear problems. Computer Methods in Applied Mechanics and Engineering 43, 251–276.

Blachut, J., Galletly, G.D., James, S., 1996. On the plastic buckling paradox for cylindrical shells. Proc. Instn. Mech. Engrs 210, 477.

Budiansky, B., 1974. Theory of buckling and postbuckling behavior of elastic structures. Advances in Applied Mechanics 14, 1–65.

Bushnell, D., 1982. Plastic buckling. In: Zamrik, S.Y., Dietrich, D. (Eds.), Pressure Vessels and Piping: Design Technology 1982, A Decade of Progress, Book No. G00213. ASME, New York, pp. 47–117.

Christofersen, J., Hutchinson, J.W., 1979. A class of phenomenological corner theories of plasticity. J. Mech. Phys. Solids 27, 465–487.

El-Ghazaly, H.A., Sherbourne, A.N., 1985. Flow and deformation theories for plate plastic buckling — an engineering approach. Solid Mechanics Archives 10, 257–287.

Giezen, J.J., 1988. Plastic buckling of cylinders under biaxial loading. Ph.D. thesis. California Institute of Technology, Pasadena, CA, February 1988.

Hecker, S.S., 1976. Experimental studies of yield phenomena in biaxially loaded metals. In: Constitutive Equations in Viscoplasticity, AMD-Vol. 20. ASME, New York, pp. 1–33.

Hutchinson, J.W., 1973. Finite strain analysis of elastic–plastic solids and structures. In: Hartung, R.F. (Ed.), Numerical Solution of Nonlinear Structural Problems. ASME, New York, p. 17.

Hutchinson, J.W., 1974. Advances in Applied Mechanics, vol. 14. Academic Press, New York, p. 67.

Koiter, W.T., 1945. The stability of elastic equilibrium. Thesis, Technische Hooge School at Delft (in Dutch), English Translation: Technical Report No. AFFDL-TR-70-25, Sponsored by Lockheed Missiles and Space Co., February 1970.

Mikkelsen, L.P., 1995. Elastic–viscoplastic buckling of circular cylindrical shells under axial compression. Eur. J. Mech., A/Solids 14 (6), 901–920.

Mikkelsen, L.P., 1996. Axisymmetric collapse of viscoplastic cylindrical shells under axial compression. Report No. 537, Danish Center for Applied Mathematics and Mechanics, Technical University of Denmark, DK-2800 Lyngby, Denmark, December 1996.

Needleman, A., Tvergaard, V., 1977. Necking of biaxially stretched elastic–plastic circular plates. J. Mech. Phys. Solids 25, 159–183.

Needleman, A., Tvergaard, V., 1982. Aspects of plastic post-buckling behaviour. In: Hopkins, H.G., Sewell, M.J. (Eds.), Mechanics of Solids, The Rodney Hill 60th Anniversary Volume. Pergamon Press, London, pp. 453–498.

Peek, R., 1999. Axisymmetric wrinkling of cylinders with finite strain. Journal of Engneering Mechanics (ASCE) (submitted).

Sanders, J.L., 1954. Plastic stress–strain relations based on linear loading functions. In: Naghdi, P.M. (Ed.), Proceedings of the Second U.S. National Congress of Applied Mechanics, Ann Arbor, MI, 14–18 June. ASME, New York, p. 445.

Teng, J.G., 1994. Plastic collapse at lap joints in pressurized cylinders under axial load. Journal of Structural Engineering 120 (1), 23–45.

Triantafyllidis, N., 1985. Puckering instability phenomena in the hemispherical cup test. J. Mech. Phys. Solids 33 (2), 117–139.

Triantafyllidis, N., Peek, R., 1992. On stability and worst imperfection shape in solids with nearly simultaneous eigenmodes. Int. J. Solids Structures 29 (18), 2281–2299.

Tvergaard, V., 1983. Plastic buckling of axially compressed circular cylindrical shells. Thin-Walled Structures 1, 139–163.